Comprehensive study of the ferroelectricity induced by the spin-dependent *d*-*p* hybridization mechanism in $Ba_2XGe_2O_7$ (X = Mn, Co, and Cu)

H. Murakawa,[1] Y. Onose,[2,3] S. Miyahara,[2] N. Furukawa,[2,4] and Y. Tokura[1,2,3,5]

[1]*Correlated Electron Research Group (CERG), RIKEN-ASI, Wako 351-0198, Japan*

[2]*Multiferroics Project, ERATO, Japan Science and Technology Agency (JST), c/o Department of Applied Physics, University of Tokyo, Tokyo 113-8656, Japan*

[3]*Department of Applied Physics, University of Tokyo, Tokyo 113-8656, Japan*

[4]*Department of Physics and Mathematics, Aoyama Gakuin University, Sagamihara, Kanagawa 229-8558, Japan*

[5]*Cross-Correlation Materials Research Group (CMRG), RIKEN-ASI, Wako 351-0198, Japan*

(Received 22 March 2012; published 14 May 2012)

We have investigated the magnetoelectric properties originating from the spin-dependent hybridization between transition metal (X) d orbital and ligand ion p orbitals in the noncentrosymmetric crystals $Ba_2XGe_2O_7$ (X = Mn, Co, Cu). The novel magnetic-field responses of the electric polarization observed in the staggered antiferromagnets $Ba_2MnGe_2O_7$ ($S = 5/2$) and $Ba_2CoGe_2O_7$ ($S = 3/2$) can be accounted for by the mean-field approximation based on the *d*-*p* hybridization mechanism. In the case of the $S = 1/2$ helimagnet $Ba_2CuGe_2O_7$, we have found the metamagnetic transition to the staggered spin state in the high magnetic field region and observed an electric polarization originating from the *d*-*p* hybridization mechanism. Especially, the observation of electric polarization not only in the fully spin-polarized state at high magnetic field in $Ba_2MnGe_2O_7$ but also in all the compounds, under applied external magnetic field, strongly supports the single-spin mechanism of the *d*-*p* hybridization as the origin of ferroelectricity in this class of materials. We have examined the transition-metal dependence of the polarization magnitude in $Ba_2XGe_2O_7$ in terms of the electronic configuration in d levels and found that the unquenched orbital angular momentum determines the magnitude of the electric polarization.

DOI: 10.1103/PhysRevB.85.174106 PACS number(s): 75.85.+t, 75.50.Ee, 77.80.−e

I. INTRODUCTION

Magnetically induced ferroelectricity has been attracting much attention because of its gigantic magnetoelectric coupling to achieve the mutual control of the electricity and magnetism.[1–7] As origins of the magnetically induced ferroelectricity, three mechanisms have been proposed so far. The most prevailing one is the spin-current mechanism[8] or, equivalently, the inverse Dzyaloshinskii-Moriya (DM) mechanism.[9,10] In the transverse-helical (cycloidal) spin structure, the vector spin chirality $\boldsymbol{S}_i \times \boldsymbol{S}_j$ can induce the polarization as $\boldsymbol{P} \propto \sum_{i,j} \boldsymbol{e}_{ij} \times (\boldsymbol{S}_i \times \boldsymbol{S}_j)$, where $\boldsymbol{e}_{ij}$ denotes the unit vector connecting the interacting neighbor spins $\boldsymbol{S}_i$ and $\boldsymbol{S}_j$. The second mechanism is the magnetostriction caused by the symmetric exchange interaction $J\boldsymbol{S}_i \cdot \boldsymbol{S}_j$. The net polarization due to the magnetostriction may be finite in the magnetic structure with the multiple inequivalent magnetic sites.[11]

The third mechanism is caused by the variation of the hybridization between transition-metal d orbital and ligand p orbitals, depending on the spin moment direction of transition metal.[12,13] While the polarization is relevant to the spin-spin correlation in the former two mechanisms, a single spin moment is essential for the generation of the local electric dipole moment between the transition metal and ligand ions in this mechanism. The ferroelectricity in the proper screw structure in $CuFeO_2$[14] and in the 120° spin structure in $CuCrO_2$[15] were explained by the *d*-*p* hybridization mechanism.[16] Nevertheless, the ligand oxygen in these materials neighbors three transition metals; therefore the sum of the induced moments relevant to one ligand oxygen depends on the directions of the neighboring three magnetic moments in these systems.

Recently, we have investigated a simpler system, $Ba_2CoGe_2O_7$, in which the CoO_4 tetrahedra are connected by the nonmagnetic Ge ions. The unique variation of the polarization critically depending on the direction and magnitude of the external magnetic field in $Ba_2CoGe_2O_7$[17,18] can be well reproduced by the simple calculation based on the spin-dependent *d*-*p* hybridization mechanism,[20,21] owing to its simple magnetic and crystal structures. The magnetoelectric coupling is also valid in the teraheltz regime, and gives rise to the gigantic nonreciprocal directional dichroism.[22–24] Nevertheless, the number of materials showing the ferroelectricity due to the *d*-*p* hybridization mechanism and the evidences for the working hypothesis of this mechanism are still limited.

In this paper, in order to further examine the *d*-*p* hybridization mechanism, we have systematically investigated the magnetoelectric response in three isostructural compounds: $Ba_2MnGe_2O_7(S = 5/2)$, $Ba_2CoGe_2O_7(S = 3/2)$, and $Ba_2CuGe_2O_7(S = 1/2)$. We have newly observed the ferroelectricity in the staggered antiferromagnetic state in $Ba_2MnGe_2O_7$. The magnetic-field variation of electric polarization can be reproduced by the mean-field calculation of the ferroelectricity relevant to the spin-dependent *d*-*p* hybridization mechanism similarly to the case of $Ba_2CoGe_2O_7$. The finite polarization not only in the fully spin-polarized state in $Ba_2MnGe_2O_7$ but also in the partially spin-polarized states for all the compounds under a magnetic field suggest the *d*-*p* hybridization mechanism as the origin of the magnetoelectric response in this class of materials. In $Ba_2CuGe_2O_7$, we have found the metamagnetic transition to the staggered antiferromagnetic state and the electric polarization due to the *d*-*p* hybridization mechanism therein, indicating the validity of this mechanism even for the quantum $S = 1/2$ spin systems.

We have also investigated the transition metal dependence of the polarization in this system in the light of the spin-orbit coupling strength.

II. EXPERIMENTAL

Single crystals of $Ba_2XGe_2O_7$ (X = Mn, Co, Cu) were grown by the floating zone method in flowing oxygen gas with the growth speed of 0.5 mm/hour. The crystal axis were determined by the Laue x-ray photograph. The crystals were cut in such a way that the largest surface is orthogonal to the [001] direction. The dc magnetization measurement was performed with use of the vibrating-sample magnetometer. For the electric polarization measurement, electrodes were attached to the (001) surfaces. The electric polarization was deduced by the time-integral of the observed displacement current $I_d = dP/dt$. The H and T dependencies of the electric polarization were obtained by measuring I_d, while changing H at a rate of 10^{-2} T/s and increasing T at 2 K/s, respectively.

III. CRYSTAL STRUCTURE AND MAGNETISM OF $Ba_2XGe_2O_7$ (X = Mn, Co, Cu)

Figures 1(a) and 1(b) illustrate the crystal structure of $Ba_2XGe_2O_7$. The space group has been reported to be $P\bar{4}2_1m$,[25] which is tetragonal and noncentrosymmetric but nonpolar. The crystal structure is composed of the corner shared XO_4 and GeO_4 tetrahedra, and intervening Ba ions. There are two inequivalent XO_4 tetrahedra, of which the lower-lying oxygen bond, are tilted by the angle $\pm\kappa$ from [110] as shown in Fig. 1(b). The recent structural analysis reports $\kappa \sim 24^\circ$ for $Ba_2CoGe_2O_7$,[26] while there are no published values of κ for X = Mn and Cu.

Figures 1(c)–1(e) show the electronic structure of the transition-metal d orbital state in $Ba_2XGe_2O_7$ (X = Mn, Co, Cu). Neglecting the tetragonal distortion of XO_4 tetrahedra, the d level is split into triply degenerated t_{2g} states and doubly degenerated e_g states. For $Ba_2MnGe_2O_7$, the d orbitals of the manganese site shows the high-spin configuration with $S = 5/2$ due to the strong Hund's rule coupling [see Fig. 1(c)]. In the case of $X = Co^{2+}$ and Cu^{2+}, $S = 3/2$ and $S = 1/2$ states are realized following the Hund's rule as shown in Figs. 1(d) and 1(e), respectively.

The antiferromagnetic superexchange interaction works between the neighboring transition metal spin moments. In addition, there exists the Dzyaloshinskii-Moriya (DM) interaction $\boldsymbol{D}\cdot(\boldsymbol{S}_i \times \boldsymbol{S}_j)$ between the nearest neighboring sites because of the lack of the local inversion symmetry.[27,28] According to the Moriya's rule,[28] there are the uniform in-plane component of DM vector $\boldsymbol{D}_{ab}\|[110]$, and the staggered out-of-plane component $\boldsymbol{D}_c\|[001]$ for the in-plane neighboring X-X bonds. The effective spin Hamiltonian is well expressed as

$$\mathcal{H} = \sum_{\text{n.n.}} J\ \boldsymbol{S}_i\cdot\boldsymbol{S}_j + \sum_{\text{i.l.}} J_c\ \boldsymbol{S}_i\cdot\boldsymbol{S}_j + \sum_i \Lambda\left(S_i^c\right)^2 + \sum_{\text{n.n.}}(\boldsymbol{D}_{ab}+\boldsymbol{D}_c)\cdot(\boldsymbol{S}_i\times\boldsymbol{S}_j), \qquad (1)$$

where Λ indicates the uniaxial magnetic anisotropy terms.

When the easy-plane type magnetic anisotropy is strong enough, the staggered antiferromagnetic state is realized. This

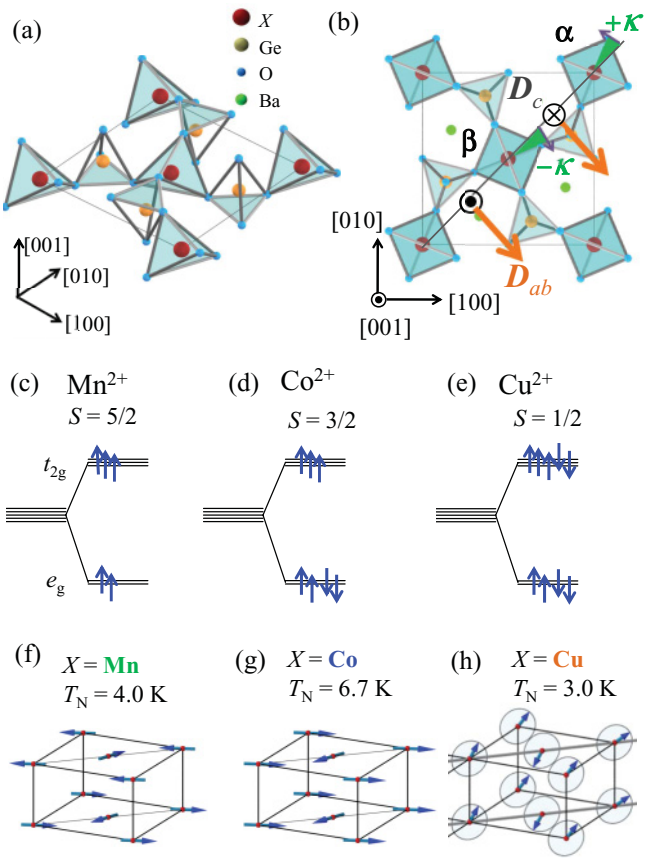

FIG. 1. (Color online) (a) Three-dimensional view and (b) top view of the crystal structure of $Ba_2XGe_2O_7$. Two types of the XO_4 tetrahedron (α and β) tilt $\pm\kappa$ from the [110] directions. In-plane and out-of-plane components of the DM vector ($\boldsymbol{D}_{ab}$ and $\boldsymbol{D}_c$) exist in this crystal structure, (c)–(e) the electronic structure of d levels in (c) $Ba_2MnGe_2O_7$, (d) $Ba_2CoGe_2O_7$, and (e) $Ba_2CuGe_2O_7$, respectively. (f)–(h) The magnetic structure of (f) $Ba_2MnGe_2O_7$, (g) $Ba_2CoGe_2O_7$, and (h) $Ba_2CuGe_2O_7$ at zero magnetic field.

is the case for $Ba_2MnGe_2O_7$ and $Ba_2CoGe_2O_7$. The staggered antiferromagnetic order is certainly realized in the (001) plane below $T_N = 4$ K in $Ba_2MnGe_2O_7$[29] and 7 K in $Ba_2CoGe_2O_7$.[30] The interplane magnetic coupling is antiferromagnetic for $Ba_2MnGe_2O_7$ ($J_c > 0$) and ferromagnetic for $Ba_2CoGe_2O_7$ ($J_c < 0$) as shown in Figs. 1(f) and 1(g), respectively. The slight canting due to the staggered $\boldsymbol{D}_c$ induces a weak ferromagnetism in $Ba_2CoGe_2O_7$, while the canted direction in a $MnGe_2O_7$ layer is opposite to that of the neighboring layer and there is no net ferromagnetic moment in $Ba_2MnGe_2O_7$ [see Figs. 1(f) and 1(g)]. On the other hand, in $Ba_2CuGe_2O_7$, the $S = 1/2$ moments on the Cu site are not affected by the uniaxial anisotropy, and thus the uniform $\boldsymbol{D}_{ab}$ gives rise to the transverse helical spin structure below $T_N = 3$ K [see Fig. 1(h)].[31]

IV. RESULTS AND DISCUSSION

Figures 2(a)–2(c) show the temperature dependencies of the magnetization, displacement current, and the corresponding electric polarization for (a) $Ba_2MnGe_2O_7$, (b) $Ba_2CoGe_2O_7$, and (c) $Ba_2CuGe_2O_7$, respectively. The measurements have

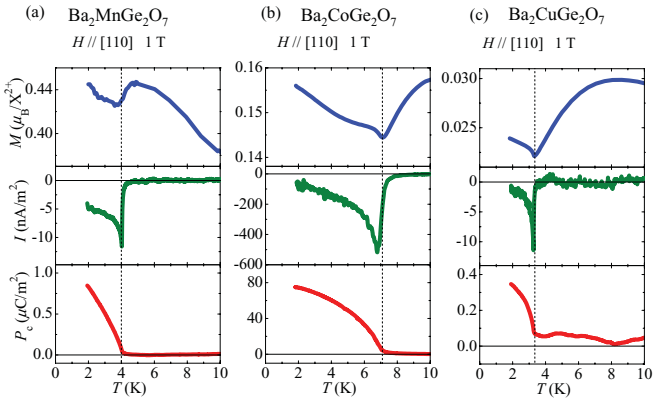

FIG. 2. (Color online) (a)–(c) The observed magnetization (upper panel), displacement current (middle panel), and the polarization (lower panel) for (a) $Ba_2MnGe_2O_7$, (b) $Ba_2CoGe_2O_7$, and (c) $Ba_2CuGe_2O_7$ measured at $H = 1$ T applied along the [110] direction.

been performed at $H = 1$ T applied along the [110] direction. The antiferromagnetic transition temperatures T_N are indicated by the vertical dotted lines: $T_N = 4$, 7, and 3 K for $X =$ Mn, Co, and Cu, respectively. The magnetization takes a cusplike minimum at T_N and turns to increase below T_N. As the characteristic properties of this class of materials, electric polarization can be induced only by applying magnetic field even without any poling procedure with electric field.[20,32] The electric polarization is shown in the lower panel of Figs. 2(a)–2(c), which is deduced by the time integration of the observed displacement current ($I_d = dP/dt$). At $H = 1$ T, the electric polarizations begin to rapidly grow below T_N. In the following sections, we study the magnetic-field response of the electric polarization on each material and show that the ferroelectricity in these materials originates from the d-p hybridization mechanism.

In the d-p hybridization mechanism, the ionic charge at the ligand site (Δe) varies as $\Delta e \propto (\boldsymbol{S}\cdot\boldsymbol{r})^2$, where $\boldsymbol{r}$ is the vector connecting the transition metal and ligand ions, owing to the spin-orbit interaction.[12,13] As a result, the local electric dipole moment $\boldsymbol{P} \propto (\boldsymbol{S}\cdot\boldsymbol{r})^2\boldsymbol{r}$ is induced along the bonding direction. Therefore, in the case of an XO_4 tetrahedron, a local electric polarization can be expressed as

$$\boldsymbol{P} \propto \sum_{l=1}^{4} (\boldsymbol{S}\cdot\boldsymbol{r}_l)^2\boldsymbol{r}_l, \tag{2}$$

where, $\boldsymbol{r}_l$ is the bonding vector between the transition metal and the lth oxygen ion [see Fig. 3(a)]. When the spin moment $\boldsymbol{S}$ is parallel to the upper-lying oxygen bond O_1-O_2, the electric dipole moment is along [001] [see Fig. 3(b)]. The electric dipole moment is unchanged after a 180° rotation of $\boldsymbol{S}$ but it can be reversed by a 90° rotation of $\boldsymbol{S}$ around the [001] axis [see Fig. 3(c)]. These are the fundamental relations to explain the observed magnetic-field response of the polarization in $Ba_2XGe_2O_7$ ($X =$ Mn, Co, Cu) as described below.

A. $Ba_2CoGe_2O_7$

At first, as a typical example of this class of ferroelectric materials, we review the in-plane magnetic-field direction

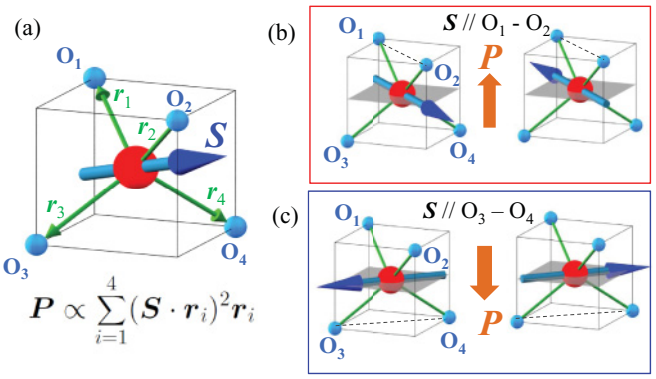

FIG. 3. (Color online) (a) Coordination of the spin moment in an XO_4 tetrahedron ($X =$ Mn, Co, Cu). (b) and (c) The relations between the spin moment and the induced polarization in a XO_4 tetrahedron.

dependence of the electric polarization in $Ba_2CoGe_2O_7$.[20] As noted above, the staggered spin structure is realized below $T_N = 7$ K with the spin moments lying in the (001) plane.[30] Even in this magnetically ordered state, there are only two inequivalent Co sites as shown in Fig. 1(g).

Figure 4(b) shows the variations of electric polarization along the c axis (P_c) with changing H between ±14 T along three characteristic in-plane directions ([110],[100], and [1$\bar{1}$0]) at 4 K. While the in-plane magnetic anisotropy is quite small as shown in Fig. 4(a), the magnitude and sign of P_c critically depend on the H direction; P_c is induced under $H \parallel [110]$ and the direction of the electric polarization is reversed under $H \parallel [1\bar{1}0]$, while P_c vanishes for $H \parallel [100]$. P_c is unchanged by the H reversal.

This H-directional variation can be well explained in terms of the spin-dependent d-p hybridization mechanism. By introducing the oxygen coordinate $\boldsymbol{r}_i$ of the two types of the XO_4 tetrahedra (see Appendix) into $\boldsymbol{P} \propto \sum_i (\boldsymbol{S}_i\cdot\boldsymbol{r}_i)^2\boldsymbol{r}_i$, each components of the induced polarization are calculated to be

$$p_i^a = A_a\left[\sin(2\kappa_i)S_i^cS_i^a - \cos(2\kappa_i)S_i^bS_i^c\right], \tag{3}$$

$$p_i^b = -A_a\left[\sin(2\kappa_i)S_i^bS_i^c - \cos(2\kappa_i)S_i^cS_i^a\right], \tag{4}$$

$$p_i^c = A_c\left\{\sin(2\kappa_i)\left[\frac{\left(S_i^a\right)^2 - \left(S_i^b\right)^2}{2}\right] - \cos(2\kappa_i)S_i^aS_i^b\right\}, \tag{5}$$

where A_a and A_c are the coupling constant of the respective components. Obviously from Eqs. (3)–(5), only the c component of the electric polarization is nonzero for the spins on the (001) plane. Next, we proceed to show the relation between the sign or the magnitude of P_c and the H direction. In $Ba_2CoGe_2O_7$, there are two magnetic sublattices (A and B), on which spin moments are represented as

$$\boldsymbol{S}_A = (S\sin(\phi+\phi_0), -S\cos(\phi+\phi_0), 0), \tag{6}$$

$$\boldsymbol{S}_B = (-S\sin(\phi-\phi_0), S\cos(\phi-\phi_0), 0), \tag{7}$$

where ϕ and ϕ_0 are an angle between [100] and the H direction, and a canting angle of the spins from the direction perpendicular to H, respectively [see Figs. 4(d)–4(f)]. The degeneracy of the location of the magnetic sublattices (A and B) on two inequivalent CoO_4 tetrahedra(α and β) is lifted due

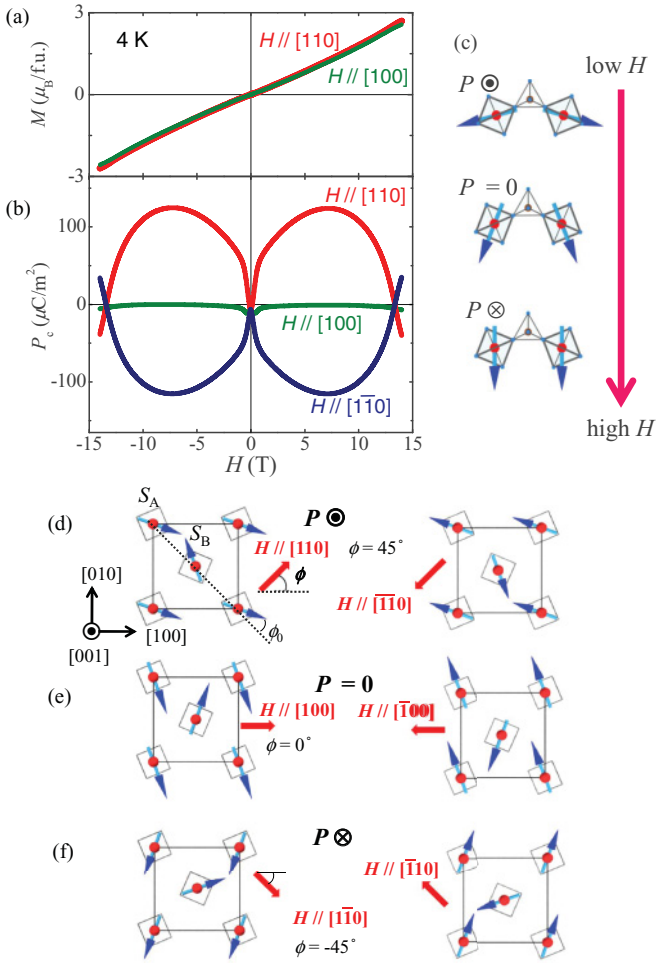

FIG. 4. (Color online) Variations of (a) magnetization and (b) out-of-plane component of the electric polarization (P_c) of $Ba_2CoGe_2O_7$ in H along several directions in the (001) plane at 4 K. (c) Illustration of the spin-structural change with increasing magnetic field along [110]. The magnetic moments are almost perpendicular to the H direction in low H, while they are aligned along the H direction in high H. The polarization shows a sign change in the course of the spin structural change. (d)–(f) Canted antiferromagnetic structure and the sign of the induced polarization P in the low magnetic field with the respective in-plane directions: (d) $H \parallel [110]$, $[\bar{1}10]$, (e) $H \parallel [100]$, $[\bar{1}00]$, and (f) $H \parallel [1\bar{1}0]$, $[\bar{1}10]$.

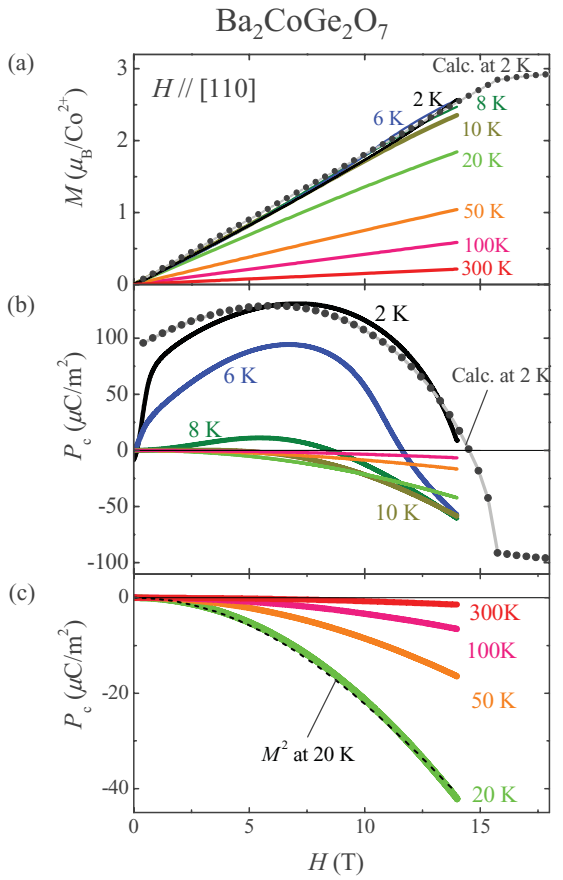

FIG. 5. (Color online) Variations of (a) magnetization, P_c in (b) the antiferromagnetically ordered and (c) the paramagnetic state in H along [110] at various temperatures in $Ba_2CoGe_2O_7$. The dots connected with the gray line in (b) is the calculated result by the mean-field approximation at 2 K. The dotted line in (c) shows the magnetic-field dependence of M^2 at 20 K.

to $\boldsymbol{D}_c$ [see Fig. 1(b)] and the staggered spin structure with A on α and B on β is unambiguously realized in $Ba_2CoGe_2O_7$ as shown in Figs. 4(d)–4(f). By introducing Eqs. (6) and (7) into Eq. (5), P_c turns out to be

$$P_c \propto \sin 2\phi \cos(2\kappa - 2\phi_0). \tag{8}$$

This clearly explains the H-direction variation of P_c, and is also consistent with the symmetry analysis; the point group of the magnetic structure in Fig. 4(d) is $mm2$, which allows the emergence of the electric polarization along the [001] direction, which is reversed by the 90° rotation around the [001] axis.

A more convincing evidence for the d-p hybridization mechanism is the characteristic variations of P_c as a function of the magnitude of $H \parallel [110]$ ($[1\bar{1}0]$): the P_c increases (decreases) with H in the low-H region below 7 T and then begins to decrease (increase) and shows the sign change at around 13 T, where the magnetization nearly saturates [see Fig. 4(a)]. This P_c variation can also be explained in terms of the d-p hybridization mechanism. In the course of the spin-orientation change from the low-H staggered antiferromagnetic ($\phi_0 = 0°$) to the high-H parallel spin ferromagnetic state ($\phi_0 = 90°$) [see Eq. (8) and Fig. 4(c)], the polarization induced by the d-p hybridization mechanism is expected to show a downturn and a sign change, being consistent with the experimental observation. As shown in Fig. 5(b), the observed P_c variation as a function of the magnitude of $H \parallel [110]$ at 2 K can be well reproduced by the result in the mean-field approximation, where we obtain $\tilde{J} = 4J + 2J_c = 0.32$ meV under the assumption $g = 2$ and $\kappa = \pi/8$. Even a clearer sign change and saturation of negative polarization are observed also in $Ba_2MnGe_2O_7$, as shown later.

For further understanding of essential magnetoelectric properties originating from the spin-dependent d-p hybridization mechanism, we show the magnetic-field (H) dependence of P_c up to 14 T along [110] at various temperatures in Figs. 5(b) and 5(c), and the corresponding magnetization M variations in Fig. 5(a). The magnetic field for the sign change in P_c decreases with approaching T_N. Even above T_N, the

P_c is finite and shows quadratic magnetic-field dependence. This is another supporting evidence for the scenario of the spin-dependent d-p hybridization mechanism because of the following reasoning: under the magnetic field $H \| [110]$ at $T > T_N$, the averaged magnetic moment $\langle S \rangle$ is aligned to H: $\phi = 45^\circ$ and $\phi_0 = 90^\circ$ in Eqs. (6) and (7), which leads the electric polarization along c as

$$\langle P_c \rangle = -K \langle S \rangle^2 \cos 2\kappa. \quad (9)$$

Thus P_c is expected to show the quadratic H dependence in the high-temperature paramagnetic region, in which M is proportional to H. Such a feature is indeed consistent with our experimental observations at $T = 20$, 50, 100, and 300 K shown in Fig. 5(c), although the magnitude of P_c is much smaller than that below T_N owing to the thermal agitation on the spins.

Finally, let us note a discrepancy between experimentally observed P_c and calculated P_c in $H \sim 0$ region; the P_c decreases steeply with decreasing H toward $H = 0$, while the calculated polarization remains finite at $H = 0$. One of the possible origins is that the polarization spontaneously forms a multidomain structure to minimize the electrostatic potential in the low-H region. As the other possibility, Romhányi *et al*. recently proposed a scenario that the antiferroelectric state is stabilized owing to the coupling between the electric polarizations.[33] Further investigation on the magnetic structure in the low-H region is required to clarify the problem.

B. $Ba_2MnGe_2O_7$

$Ba_2MnGe_2O_7$ also shows the staggered antiferromagnetic structure below $T_N = 4$ K with the spin moment lying in the (001) plane.[29] The important difference from $Ba_2CoGe_2O_7$ is the larger spin moment and Zeeman energy gain. As shown below, we could achieve the fully spin-polarized state at high magnetic field at low temperature and observe the ferroelectric polarization there, which firmly evidences the single-spin mechanism of the d-p hybridization model. The other differences are in the antiferromagnetic interlayer magnetic interaction and four inequivalent magnetic sites in the magnetic unit cell as shown in Fig. 1(f); the magnetic $A(B)$ sublattice is located on the $\alpha(\beta)$-tetrahedron in one layer, but the opposite configuration, namely B on α and A on β, is realized in the neighboring layer.

Figure 6(a) shows the magnetic-field dependence of magnetization with various magnetic field directions at 1.8 K. The in-plane magnetic anisotropy is tiny as in $Ba_2CoGe_2O_7$. The magnetic transition field H_S between the canted antiferromagnetic to the induced ferromagnetic state can be observed as the sharp peak in the susceptibility (dM/dH) curve at 8.2 T [see Fig. 6(a)]. Figure 6(b) shows the variation of P_c obtained in H along [110], [100], and [1$\bar{1}$0]. As is the case in $Ba_2CoGe_2O_7$, the electric polarization is induced along the [001] direction under $H \| [110]$, and is reversed for $H \| [1\bar{1}0]$, and vanishes in the case of $H \| [100]$. This is the first observation of ferroelectricity in this material. The magnitude of the electric polarization is two orders of magnitude smaller than that in $Ba_2CoGe_2O_7$. The difference of the magnitude of the polarization is closely related to the electronic configuration of the d levels, as discussed later.

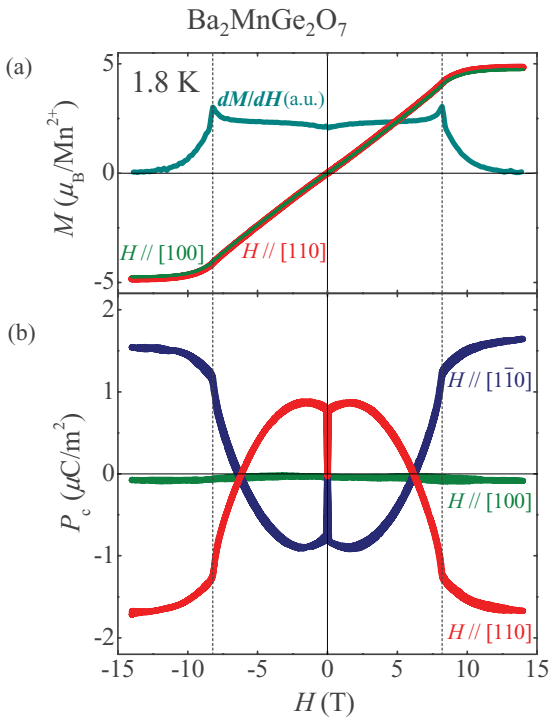

FIG. 6. (Color online) (a) Variations of magnetization in H along the [110] and [100] directions at 1.8 K for $Ba_2MnGe_2O_7$. The field-derivative of M, dM/dH in $H \| [110]$ is also shown. (b) Variations of the [001] component of the electric polarization (P_c) in H along [110], [100], and [1$\bar{1}$0] at 1.8 K.

Thanks to the achievable magnetization-saturation field ($H_S \sim 8.2$ T), the variation of P_c can be observed in the entire spin-reorientation process under H from the staggered ($\phi_0 = 0^\circ$) to the completely parallel spin state ($\phi_0 = 90^\circ$). With increasing H along [110], P_c shows slight increase up to 1.8 T and then decreases. At 6.2 T, P_c changes the sign and shows kink at $H_S = 8.2$ T, corresponding to the magnetic transition. The observation of the finite electric polarization in the fully spin-polarized ferromagnetic state in the high magnetic field is a strong evidence for the d-p hybridization mechanism because the other mechanisms of the magnetically induced ferroelectricity are irrelevant in this magnetic state. While the magnetic field variation of ferroelectricity is qualitatively similar to that in $Ba_2CoGe_2O_7$, it should be noted that the shape of the P-H curve is slightly different, reflecting the inequivalent magnetic sites generated by the interplane antiferromagnetic interaction. The polarization induced by the other type of the spin configuration (B on α and A on β) is expressed just by replacing κ to $-\kappa$ in Eq. (8), resulting in

$$P_c \propto \sin 2\phi \cos(2\kappa + 2\phi_0). \quad (10)$$

Thus the total polarization is proportional to the summation of Eqs. (8) and (10) as

$$P_c \propto \sin(2\phi)\ \cos(2\phi_0)\ \cos(2\kappa). \quad (11)$$

As shown in Fig. 7(b), the polarization variation observed in $Ba_2MnGe_2O_7$ with $H \| [110]$ at 1.8 K can also be roughly reproduced by the mean-field approximation in Eq. (11) with the parameter $\tilde{J} = 0.11$ meV, $g = 2$,[29] and $\kappa = \pi/8$. In this

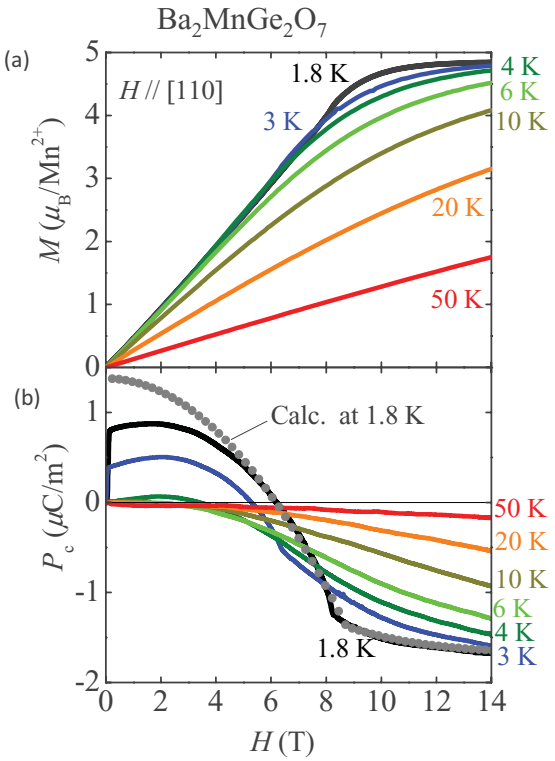

FIG. 7. (Color online) Variations of (a) magnetization and (b) P_c in H along [110] at various temperatures in $Ba_2MnGe_2O_7$. Closed circles represent the calculated polarization at 1.8 K deduced by the mean-field approximation.

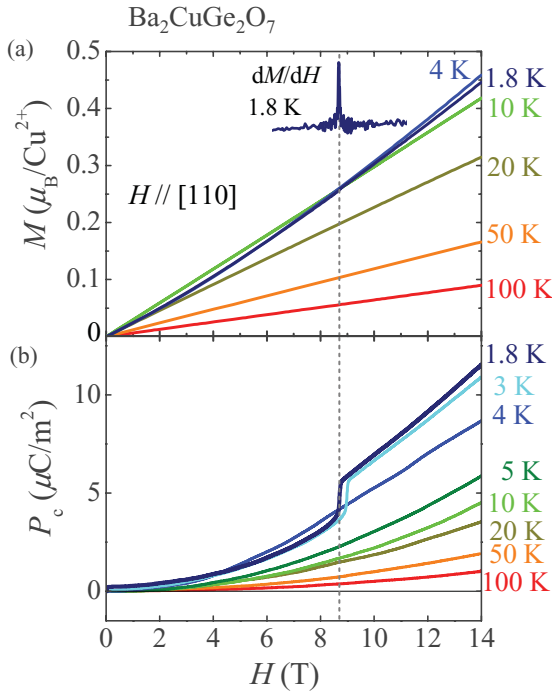

FIG. 8. (Color online) Variations of (a) magnetization and (b) P_c in H along [110] at various temperatures in $Ba_2CuGe_2O_7$.

case, the deviation between the observed P_c and the calculation is larger in the low-field region. Judging from the ratio of the measured temperature (2 K for $Ba_2CoGe_2O_7$ and 1.8 K for $Ba_2MnGe_2O_7$) to the transition temperature ($T_N = 7$ K for $Ba_2CoGe_2O_7$ and 4 K for $Ba_2MnGe_2O_7$), the effect of the thermal fluctuation is so strong that the mean-field description is not so valid especially in the low-field regime in the case of $Ba_2MnGe_2O_7$. The origin of the sudden disappearance of P_c below 0.05 T is considered to be of the same origin as in the case of $Ba_2CoGe_2O_7$. Figures 7(a) and 7(b) show the H dependencies of M and P_c ($H \parallel [110]$) at various temperatures. As in $Ba_2CoGe_2O_7$, the electric polarization is induced by the external magnetic field even above $T_N = 4$ K; $P_c \propto H^2$ in the high-temperature region. The temperature and magnetic-field dependencies can again be explained well by the spin-dependent d-p hybridization mechanism.

C. $Ba_2CuGe_2O_7$

In contrast to the in-plane staggered antiferromagnets $Ba_2CoGe_2O_7$ and $Ba_2MnGe_2O_7$, the helical spin structure [see Fig. 1(h)] is realized in $Ba_2CuGe_2O_7$ by the uniform $\boldsymbol{D}_{ab}$ as the DM-induced modulation of the staggered antiferromagnetic structure [$\boldsymbol{Q}_{AF} = (1,0,0)$] below $T_N = 3$ K.[31] In this tetragonal symmetry, two types of the modulation vectors due to the DM interaction $\Delta\boldsymbol{k}$, namely, $\Delta\boldsymbol{k} = (\xi,-\xi,0)$ or $(\xi,\xi,0)(\xi \sim 0.027)$ are possible in zero magnetic field. Therefore the magnetic propagation vector $\boldsymbol{k}$ is expressed by the sum of $\boldsymbol{Q}_{AF}$ and the modulation wave vector $\Delta\boldsymbol{k}$, namely, $\boldsymbol{k} = (1+\xi,-\xi,0)$ or $(1+\xi,\xi,0)$. After cooling down to below $T_N = 3$ K without magnetic field, both $\Delta\boldsymbol{k}$ domains exist due to the degeneracy.[30] $\Delta\boldsymbol{k}$ can be aligned to $[1\bar{1}0]$ ([110]) by applying H parallel to [110] ($[1\bar{1}0]$).[34] Previously, we have observed the electric polarization induced by the helical spin structure in $Ba_2CuGe_2O_7$ under the magnetic field up to 5 T.[32] Similarly to the cases in the staggered antiferromagnets $Ba_2CoGe_2O_7$ and $Ba_2MnGe_2O_7$, P_c is induced by applying $H \parallel [110]$ and reversed under $H \parallel [1\bar{1}0]$. Taking into account the fact that the direction of $\Delta\boldsymbol{k}$ is fixed to $[1\bar{1}0]$ ([110]) under $H \parallel [110]$ ($[1\bar{1}0]$), there is the one-to-one correspondence between the direction of $\Delta\boldsymbol{k}$ and the sign of P_c.

Here, we have performed measurements of P_c and corresponding M in the higher magnetic fields up to 14 T at various temperatures. Figure 8(b) shows the variations of P_c in H along the [110] direction up to 14 T. At the lowest temperature 1.8 K, P_c shows H^2 dependence in the low-H region and discontinuous change at around 8.7 T. Correspondingly, the susceptibility (dM/dH) shows a sharp peak as depicted in the inset of Fig. 8(a). These anomalies are also observed at 3 K at around 9 T, but disappear in the paramagnetic state above 4 K. Therefore they are considered to be caused by the metamagnetic transition from the low-H helical spin state. In the high-temperature region or the paramagnetic state, P_c shows smooth H dependence and is proportional to H^2 as is the cases with $Ba_2CoGe_2O_7$ and $Ba_2MnGe_2O_7$.

Figures 9(a) and 9(b) show the temperature dependencies of the magnetic susceptibility ($\chi = M/H$) and P_c at various magnetic fields along [110]. In the low-H region at 1 and 3 T, the helical spin transition is clearly seen at 3.3 and 3.7 K, respectively, as the peak of the susceptibility. Above 5 T, P_c and χ show discontinuous change at T_N as indicated by the triangular dots in Figs. 9(a) and 9(b), suggesting

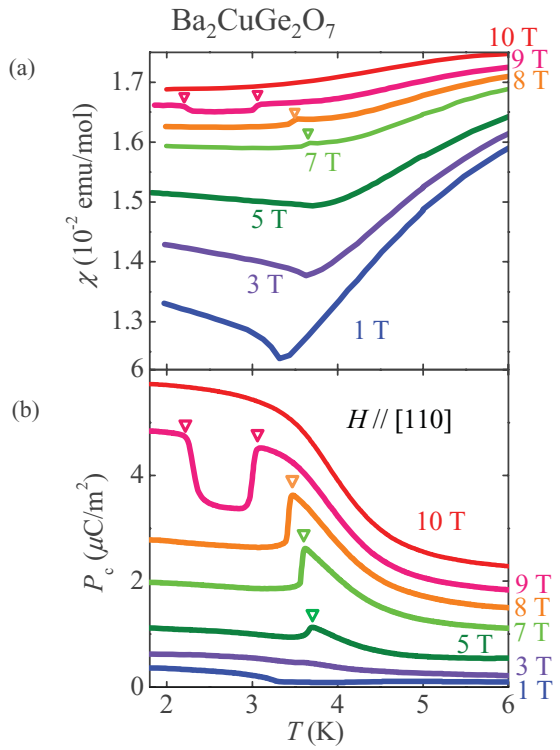

FIG. 9. (Color online) Temperature dependence of (a) magnetic susceptibility and (b) P_c at various magnitudes of H applied parallel to [110].

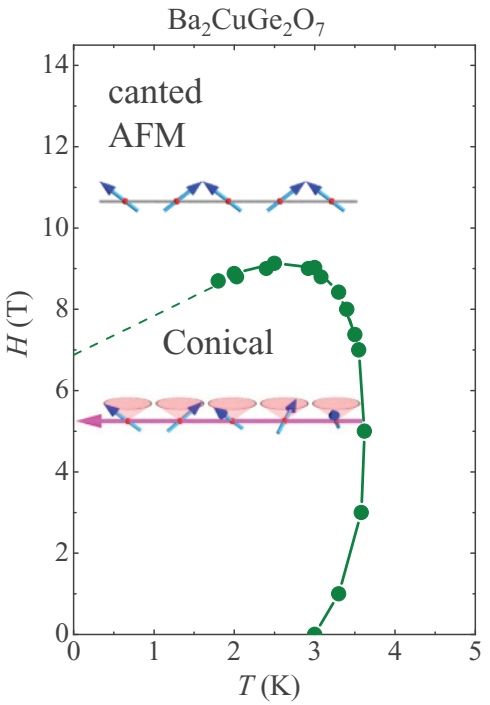

FIG. 10. (Color online) H-T phase diagram deduced from the magnetization and polarization measurements. In the low-H region, the helical (conical) spin structure is realized at low temperature. On the other hand, in the high-H region, the canted (staggered) antiferromagnetic state is stabilized.

the first-order nature of the phase transition. The reentrant transition is observed at 9 T. At 10 T, the P_c and χ do not show any anomaly and smoothly vary with decreasing temperature. Judging from the smooth connection from the paramagnetic region, the high-field magnetic phase seems to have the same magnetic symmetry as the paramagnetic state. Such a magnetic phase is the staggered antiferromagnetic state observed in $Ba_2CoGe_2O_7$. In-plane magnetic field seems to favor the staggered antiferromagnetic state. Based on these experimental results, we construct the magnetic phase diagram of $Ba_2CuGe_2O_7$ in Fig. 10. Below 9 T, the helical or the conical spin structure is realized below T_N. T_N slightly increases with increasing H up to 7 T and turns to decrease above 8 T. In the high-H region above 9 T, the magnetic transition is not detected down to 1.8 K, indicating the crossover from the paramagnetic state to the staggered antiferromagnetic state. This is consistent with the recent neutron diffraction study done by Mühlbauer *et al.*[35]

As mentioned above, the polarization in the spontaneously or field-induced spin-polarized state should be caused by the d-p hybridization mechanism. Note here, however, the right hand side of the Eq. (2) should be independent of the spin direction for $S = 1/2$ quantum spin moment. In the d-p hybridization model, the orbital angular momentum coupled to the spin moment is relevant, and therefore the "classical" approximation [see Eq. (2)] may be justified even in this quantum spin system. In other words, the experimental observation of the electric polarization in the staggered antiferromagnetic state is evidence for the validity of the d-p hybridization model even for $S = 1/2$ systems.

D. Transition-metal dependence of the polarization magnitude

Finally, we examine the transition-metal dependence of the magnitude of the polarization observed in $Ba_2XGe_2O_7$ (X = Mn, Co, and Cu) in terms of the electronic configurations in d levels. According to Eq. (5), the on-site magnetoelectric coupling strength A_c in each compound can be deduced from a slope of P_c as a function of $(M/M_S)^2$ in the paramagnetic state at much higher temperature above T_N. Here, M_S is the saturation value of magnetization in each compound. Figure 11 shows the absolute value of P_c plotted as a function of $(M/M_S)^2$ for all the compounds obtained at 50 K, well above T_N. In the case of $Ba_2CoGe_2O_7$ and $Ba_2CuGe_2O_7$, the coupling constants A_c show similar magnitude. On the other hand, it is almost two orders of magnitude smaller in the case of $Ba_2MnGe_2O_7$. In order to clarify the microscopical origin of such a large difference in the magnitude of the induced polarization, we focus on the electronic configurations of each transition metal ion. As shown in Fig. 11, in the case of Co and Cu, the ligand p orbital is dominantly hybridized with the unoccupied t_{2g} orbitals, where the spin-orbit interaction is active. On the other hand, in the case of Mn, the dominant hybridization occurs in the lower-energy unoccupied e_g orbitals, where the orbital moment is quenched and the effective spin-orbit interaction works only through the perturbation process with the higher-lying t_{2g} levels. Therefore the polarization induced by the d-p hybridization should be much smaller in $Ba_2MnGe_2O_7$ compared to those in $Ba_2CoGe_2O_7$ and $Ba_2CuGe_2O_7$, as observed.

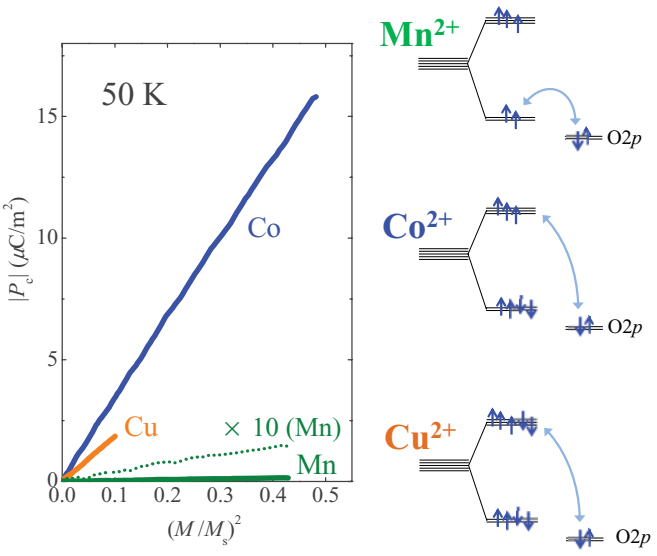

FIG. 11. (Color online) P_c at 50 K plotted against $(M/M_S)^2$ for $Ba_2XGe_2O_7$ (X = Mn, Co, Cu). M_S stands for the saturated magnetization in the high-field limit. Right panel schematically shows the low-energy hybridization between transition-metal d and ligand p levels.

V. CONCLUDING REMARKS

We have performed the systematic investigation of the magnetically-induced polarization in the noncentrosymmetric crystal antiferromagnets $Ba_2XGe_2O_7$ (X = Mn, Co, Cu). In the case of the staggered antiferromagnets $Ba_2CoGe_2O_7$ and $Ba_2MnGe_2O_7$, the characteristic magnetic-field variation of polarization, including its sign change, can be well explained by the spin-dependent d-p hybridization mechanism. In particular, the observation of finite polarization in the fully spin-polarized state in the high-magnetic field region of $Ba_2MnGe_2O_7$ is a decisive evidence for the spin mechanism of the d-p hybridization. As another strong evidence of the spin-dependent d-p hybridization mechanism, we have shown that the polarization is produced by the magnetic-field induced partial magnetization even in the paramagnetic state in all the compounds. This is also true for in the quantum spin system $Ba_2CuGe_2O_7$ in which the polarization due to the hybridization mechanism is observed. We have also investigated the transition metal dependence of the polarization magnitude and found that the hybridization between oxygen p and t_{2g} orbitals with unquenched orbital angular momentum produces relatively large electric polarization for $Ba_2CoGe_2O_7$ and $Ba_2CuGe_2O_7$, while the polarization is small for $Ba_2MnGe_2O_7$, in which the orbital quenched e_g orbital is responsible for the d-p hybridization. Thus the d-p hybridization mechanism can comprehensively explain the magnetoelectric phenomena in this class of materials.

ACKNOWLEDGMENTS

The authors thank T. Arima and Y. Tokunaga for the fruitful discussions and the experimental support. This work was in part supported by a Grant-In-Aid for Science Research from the Ministry of Education, Culture, Sports, Science and Technology (Grant Nos. 20046004, 20340086, 19684011, 22014003, and 23684023), and by Funding Program for World-Leading Innovative R&D on Science and Technology (FIRST Program), Japan.

APPENDIX: CALCULATION

1. Model Hamiltonian

The magnetic behaviors in Néel ordered states of $Ba_2XGe_2O_7$ (X = Mn and Co) can be reproduced well by a simple Heisenberg model:[29,30]

$$\mathcal{H} = \sum_{\text{n.n.}} J\ \boldsymbol{S}_i \cdot \boldsymbol{S}_j + \sum_{\text{i.l.}} J_c\ \boldsymbol{S}_i \cdot \boldsymbol{S}_j, \tag{12}$$

where $\boldsymbol{S}_i$ is an $S = 5/2$ (3/2) operator on the i site when X = Mn (Co). Here, J is an intra-layer nearest-neighbor interactions and J_c is an interlayer coupling. J (>0) is fixed to be an antiferromagnetic interactions. J_c is an antiferromagnetic interactions for $Ba_2MnGe_2O_7$,[29] whereas ferromagnetic for $Ba_2CoGe_2O_7$.[29,30] The sum is taken for all bonds. Magnetization is defined as

$$\boldsymbol{M} = \frac{1}{N}\sum_{i=1}^{N} g\boldsymbol{S}_i, \tag{13}$$

where N is a number of spins. Under the external magnetic field $\boldsymbol{H} = (H\cos\phi, H\sin\phi, 0)$, two-sublattice magnetic ordered state is stabilized as a ground state for X = Mn and Co. However, ordering structures of the sublattices depend on X, i.e., a sign of J_c, as noted in the main text. G-type structure is realized when X = Mn [see Fig. 1(f)] and C-type structure when X = Co [see Fig. 1(g)], respectively. The spin structures on A and B sublattices are represented as

$$\boldsymbol{S}_A = (S\sin(\phi+\phi_0), -S\cos(\phi+\phi_0), 0), \tag{14}$$

$$\boldsymbol{S}_B = (-S\sin(\phi-\phi_0), S\cos(\phi-\phi_0), 0), \tag{15}$$

where ϕ_0 is a canting angle of the spins and thus the magnetization along field is $M = gS\sin\phi_0$ [see Figs. 4(d)–4(f)]. Under $\boldsymbol{H}$, the ground state is twofold degenerate. When a state with $\phi_0 (0 < \phi_0 < \pi/2)$ in Eqs. (14) and (15) is one of the ground states, the other state is given by the transformation $\phi_0 \to \pi - \phi_0$.

To describe the coupling between electric polarizations and spin structures, we introduce a spin-dependent electric polarization. On XO_4 cluster, the electric dipole moment owing to d-p hybridization mechanism is described as

$$\boldsymbol{P} = \frac{K}{d^3}\sum_{l=1}^{4}(\boldsymbol{S}\cdot\boldsymbol{r}_l)^2\,\boldsymbol{r}_l. \tag{16}$$

K is a constant in a unit of C m, d^3 is a volume of a cube that contains the tetrahedron, and $\boldsymbol{r}_l$ is a vector that connects a spin site and a ligand atom [see also Fig. 3(a)] :

$$\boldsymbol{r}_1 = \left(-\frac{d}{2}(\cos\kappa_i + \sin\kappa_i), \frac{d}{2}(\cos\kappa_i - \sin\kappa_i), \frac{d}{2}\right), \tag{17}$$

$$\boldsymbol{r}_2 = \left(\frac{d}{2}(\cos\kappa_i + \sin\kappa_i), -\frac{d}{2}(\cos\kappa_i - \sin\kappa_i), \frac{d}{2}\right), \tag{18}$$

$$\boldsymbol{r}_3 = \left(-\frac{d}{2}(\cos\kappa_i - \sin\kappa_i), -\frac{d}{2}(\cos\kappa_i + \sin\kappa_i), -\frac{d}{2}\right), \quad (19)$$

$$\boldsymbol{r}_4 = \left(\frac{d}{2}(\cos\kappa_i - \sin\kappa_i), \frac{d}{2}(\cos\kappa_i + \sin\kappa_i), -\frac{d}{2}\right). \quad (20)$$

Here, κ_i is a rotation angle of the XO_4 tetrahedron around the [001] axis as defined in Fig. 1(b). In the crystal, there are two inequivalent XO_4 tetrahedra owing to the rotation angles, i.e., $\kappa_i = \kappa$ on α sublattice and $\kappa_i = -\kappa$ on β sublattice. α and β sublattices are aligned to form C-type structure [see Fig. 1(b)]. Thus the magnetic unit cell in $Ba_2CoGe_2O_7$ is identical with the crystallographic unit cell, whereas that of $Ba_2MnGe_2O_7$ is double of the crystallographic one. From Eq. (16), a spin-dependent electric dipole moment at i site is derived as

$$p_i^a = K\left[\sin(2\kappa_i) S_i^c S_i^a - \cos(2\kappa_i) S_i^b S_i^c\right], \quad (21)$$

$$p_i^b = -K\left[\sin(2\kappa_i) S_i^b S_i^c - \cos(2\kappa_i) S_i^c S_i^a\right], \quad (22)$$

$$p_i^c = K\left\{\sin(2\kappa_i)\left[\frac{\left(S_i^a\right)^2 - \left(S_i^b\right)^2}{2}\right] - \cos(2\kappa_i) S_i^a S_i^b\right\}. \quad (23)$$

Obviously, from Eqs. (21)–(23), only z component of the electric polarization is nonzero for spins in the (001) plane. An electric polarization in $Ba_2XGe_2O_7$ under $\boldsymbol{H} \perp c$ is defined as

$$P_c = \frac{1}{NV}\sum_{i=1}^{N} p_i^z, \quad (24)$$

where V is a volume per X atom.

2. Mean-field approximation

We perform mean-field approximation to discuss spin moment and electric polarization at a finite temperature T.[36] Within a mean-field approximation, the Hamiltonian (12) can be approximated as

$$\mathcal{H}^{\mathrm{MF}} = \mathcal{H}_A + \mathcal{H}_B \quad (25)$$

$$= \sum_{i\subset A}\{\tilde{J}\langle \boldsymbol{S}_B\rangle - g\mu_B \boldsymbol{H}\}\cdot \boldsymbol{S}_i + \sum_{i\subset B}\{\tilde{J}\langle \boldsymbol{S}_A\rangle - g\mu_B \boldsymbol{H}\}\cdot \boldsymbol{S}_i, \quad (26)$$

where $\tilde{J} = 4J + 2J_c$. The thermodynamical average of each spin is defined as

$$\langle \boldsymbol{S}_\gamma\rangle = \frac{\mathrm{Tr}(\boldsymbol{S}_\gamma e^{-\beta\mathcal{H}_\gamma})}{\mathrm{Tr}(e^{-\beta\mathcal{H}_\gamma})}, \quad (27)$$

where $\gamma = A$ or B and $\beta = 1/k_B T$. Within a mean-field approximation, spin states under $\boldsymbol{H} \perp c$ are given by

$$\langle \boldsymbol{S}_A\rangle = (\langle S\rangle \sin(\phi+\phi_0), -\langle S\rangle\cos(\phi+\phi_0), 0), \quad (28)$$

$$\langle \boldsymbol{S}_B\rangle = (-\langle S\rangle \sin(\phi-\phi_0), \langle S\rangle\cos(\phi-\phi_0), 0), \quad (29)$$

where $\langle S\rangle \equiv |\langle S_A\rangle| = |\langle S_B\rangle|$. The canting angle ϕ_0 (see Fig. 4) is obtained from

$$2\tilde{J}\langle S\rangle \sin\phi_0 = H. \quad (30)$$

A local electric polarization $\langle p_i^c\rangle$ at i site is described as

$$\langle p_i^c\rangle = K\left[\sin(2\kappa_i)\left(\langle S_i^a\rangle^2 - \langle S_i^b\rangle^2\right) - 2\cos(2\kappa_i)\langle S_i^a\rangle\langle S_i^b\rangle\right]. \quad (31)$$

The electric polarization P_c on $Ba_2XGe_2O_7$ is derived from Eqs. (24) and (28)–(31). The results depend on stacking patterns along c directions. For $Ba_2MnGe_2O_7$ with an antiferromagnetic stacking along c, P_c is given in a form

$$\langle P_c\rangle = K\langle S\rangle^2 \sin(2\phi)\cos(2\phi_0)\cos(2\kappa). \quad (32)$$

The electric polarization (32) does not depend on the degenerate ground states since both states induces the same magnitude of the electric polarization. Note that the ground state contains four Mn sites in the unit cell, i.e., magnetic A and B sublattices locate on both α and β sublattices of the lattice structure. On the other hand, P_c for $Ba_2CoGe_2O_7$ is derived as

$$\langle P_c\rangle = K\langle S\rangle^2 \sin(2\phi)\cos 2(\phi_0 - \kappa) \quad (33)$$

for one of ground states with ϕ_0, i.e., magnetic $A(B)$ sublattice locate on $\alpha(\beta)$ sublattice of the lattice structure, while

$$\langle P_c\rangle = K\langle S\rangle^2 \sin(2\phi)\cos 2(\phi_0 + \kappa) \quad (34)$$

for the other state with $\pi - \phi_0$, i.e., magnetic $A(B)$ sublattice locate on $\beta(\alpha)$ sublattice. For nonzero κ, the magnetic field dependence of the electric polarization strongly depends on the ground-state structures. We introduce a small DM interaction to lift the degeneracy of Néel ordered states. We choose the sign of DM interaction to realize a ground state with ϕ_0, i.e., $\langle P_c\rangle$ in Eq. (33), to reproduce the magnetic field dependence of the electric polarization when $\boldsymbol{H}\|[110]$[23,32,33] (see Sec. IV A). In Eqs. (32)–(34), the magnetic-field directional dependence is given by $\sin(2\phi)$, which is consistent with the experimental observations: $\langle P_c\rangle \neq 0$ when $\boldsymbol{H}\|[110]$ ($\phi = \pi/4$) and $\langle P_c\rangle$ vanishes under $\boldsymbol{H}\|[100]$ ($\phi = 0$).[32] As we show in the main text, the results in the simple model (12) agree well with the experimental observation.

[1] T. Kimura, T. Goto, H. Shintani, K. Ishizaka, T. Arima, and Y. Tokura, Nature (London) **426**, 55 (2003).
[2] M. Fiebig, J. Phys. D. **38**, R123 (2005).
[3] S-W. Cheong and M. Mostovoy, Nat. Mater. **6**, 13 (2007).
[4] Y. Tokura, Science **312**, 1481 (2006).
[5] T. Kimura, Annu. Rev. Mater. Res. **37**, 387 (2007).
[6] T. Arima, J. Phys. Soc. Jpn. **80**, 052001 (2011).
[7] Y. Tokura and S. Seki, Adv. Mater. **22**, 1554 (2010).
[8] H. Katsura, N. Nagaosa, and A. V. Balatsky, Phys. Rev. Lett. **95**, 057205 (2005).
[9] I. A. Sergienko and E. Dagotto, Phys. Rev. B **73**, 094434 (2006).
[10] M. Mostovoy, Phys. Rev. Lett. **96**, 067601 (2006).
[11] T. Arima, A. Tokunaga, T. Goto, H. Kimura, Y. Noda, and Y. Tokura, Phys. Rev. Lett. **96**, 097202 (2006).

[12]C. Jia, S. Onoda, N. Nagaosa, and J. H. Han, Phys. Rev. B **74**, 224444 (2006).
[13]C. Jia, S. Onoda, N. Nagaosa, and J. H. Han, Phys. Rev. B **76**, 144424 (2007).
[14]T. Kimura, J. C. Lashley, and A. P. Ramirez, Phys. Rev. B **73**, 220401(R) (2006).
[15]S. Seki, Y. Onose, and Y. Tokura, Phys. Rev. Lett. **101**, 067204 (2008).
[16]T. Arima, J. Phys. Soc. Jpn. **76**, 073702 (2007).
[17]H. T. Yi, Y. J. Choi, S. Lee, and S-W. Cheong, Appl. Phys. Lett **92**, 212904 (2008).
[18]In the isostructural compounds $Ca_2CoSi_2O_7$, similar magnetic-field responses of the polarization have been reported.[19]
[19]M. Akaki, J. Tozawa, D. Akahoshi, and H. Kuwahara, Appl. Phys. Lett. **94**, 212904 (2009).
[20]H. Murakawa, Y. Onose, S. Miyahara, N. Furukawa, and Y. Tokura, Phys. Rev. Lett. **105**, 137202 (2010).
[21]K. Yamauchi, P. Barone, and S. Picozzi, Phys. Rev. B **84**, 165137 (2011).
[22]I. Kézsmárki, N. Kida, H. Murakawa, S. Bordács, Y. Onose, and Y. Tokura, Phys. Rev. Lett. **106**, 057403 (2011).
[23]S. Miyahara and N. Furukawa, J. Phys. Soc. Jpn. **80**, 073708 (2011).
[24]S. Bordács, I. Kézmárki, D. Szaller, L. Demko, N. Kida, H. Murakawa, Y. Onose, R. Shimano, T. Room, U. Nagel, S. Miyahara, N. Furukawa, and Y. Tokura, eprint arXiv:1109.1597.
[25]A recent detailed x-ray diffraction study revealed that the slight distortion from the $P\bar{4}2_1m$ structure.[26]
[26]V. Hutanu, A. Sazonov, H. Murakawa, Y. Tokura, B. Náfrádi, and D. Chernyshov, Phys. Rev. B. **84**, 212101 (2011).
[27]I. E. Dzyaloshinskii, J. Phys. Chem. Solids **4**, 241 (1958).
[28]T. Moriya, Phys. Rev. **120**, 91 (1960).
[29]T. Masuda, S. Kitaoka, S. Takamizawa, N. Metoki, K. Kaneko, K. C. Rule, K. Kiefer, H. Manaka, and H. Nojiri, Phys. Rev. B **81**, 100402(R) (2010).
[30]A. Zheludev, T. Sato, T. Masuda, K. Uchinokura, G. Shirane, and B. Roessli, Phys. Rev. B **68**, 024428 (2003).
[31]A. Zheludev, G. Shirane, Y. Sasago, N. Koide, and K. Uchinokura, Phys. Rev. B **54**, 15163 (1996).
[32]H. Murakawa, Y. Onose, and Y. Tokura, Phys. Rev. Lett. **103**, 147201 (2009).
[33]J. Romhányi, M. Lajkó, and K. Penc, Phys. Rev. B **84**, 224419 (2011).
[34]A. Zheludev, S. Maslov, G. Shirane, Y. Sasago, N. Koide, K. Uchinokura, D. A. Tennant, and S. E. Nagler, Phys. Rev. B **56**, 14006 (1997).
[35]S. Mühlbauer, S. Gvasaliya, E. Ressouche, E. Pomjakushina, and A. Zheludev, e-print arXiv:1203.3650.
[36]K. Yoshida, *Theory of Magnetism* (Spinger-Verlag, Berlin, New York, 1996).